3D Printing of large-scale and highly porous biodegradable tissue engineering scaffolds from poly(trimethylene-carbonate) using two-photon-polymerization

Biofabrication

PAPER

3D Printing of large-scale and highly porous biodegradable tissue engineering scaffolds from poly(trimethylene-carbonate) using two-photon-polymerization

Gregor Weisgrab[1,2], Olivier Guillaume[1,2], Zhengchao Guo[3], Patrick Heimel[2,4], Paul Slezak[2,4], André Poot[3], Dirk Grijpma[3] and Aleksandr Ovsianikov[1,2]

[1] 3D Printing and Biofabrication Group, Institute of Materials Science and Technology, TU Wien Getreidemarkt 9/308, 1060, Vienna, Austria
[2] Austrian Cluster for Tissue Regeneration (http://www.tissue-regeneration.at), Vienna, Austria
[3] Department of Biomaterials Science and Technology, Faculty of Science and Technology, Technical Medical Centre, University of Twente, Enschede, The Netherlands
[4] Ludwig Boltzmann Institute for Experimental and Clinical Traumatology, BioImaging Austria/CMI, Vienna, Austria

E-mail: aleksandr.ovsianikov@tuwien.ac.at

OPEN ACCESS

RECEIVED
4 May 2020

REVISED
4 August 2020

ACCEPTED FOR PUBLICATION
4 September 2020

PUBLISHED
30 September 2020

Keywords: two-photon polymerization, poly(trimethylene carbonate), tissue engineering, scaffold, biomaterial ink

Supplementary material for this article is available online

Abstract

The introduction of two-photon polymerization (2PP) to the field of tissue engineering and regenerative medicine (TERM) has led to great expectations for the production of scaffolds with an unprecedented degree of complexity and tailorable architecture. Unfortunately, resolution and size are usually mutually exclusive when using 2PP, resulting in a lack of highly-detailed scaffolds with a relevant size for clinical application. Through the combination of using a highly reactive photopolymer and optimizing key printing parameters, we propose for the first time a biodegradable and biocompatible poly(trimethylene-carbonate) (PTMC)-based scaffold of large size (18 × 18 × 0.9 mm) with a volume of 292 mm^3 produced using 2PP. This increase in size results in a significant volumetric increase by almost an order of magnitude compared to previously available large-scale structures (Stichel 2010 *J. Laser Micro./Nanoeng.* **5** 209–12). The structure's detailed design resulted in a highly porous scaffold (96%) with excellent cytocompatibility, supporting the attachment, proliferation and differentiation of human adipose-derived mesenchymal stem cells towards their osteogenic and chondrogenic lineages. This work strongly attests that 2PP is becoming a highly suitable technique for producing large-sized scaffolds with a complex architecture. We show as a proof-of-concept that an arrayed design of repetitive units can be produced, but a further perspective will be to print scaffolds with anisotropic features that are more representative of human tissues.

1. Introduction

The use of cell-laden three-dimensional (3D) scaffolds is a common strategy in the field of tissue engineering and regenerative medicine (TERM). When recreating the architectural features of tissues, several key factors, such as biocompatibility, mechanical support and porosity play an important role for the design of a scaffold. While traditional methods, such as salt leaching, gas foaming or freeze-drying follow these rules for scaffold fabrication, they lack the spatial control over the internal architecture of the scaffold. More specifically, they do not provide any control over the resulting pores size and overall porosity of the resulting structure. Both, however, are of vast importance to a scaffold's design as they directly affect nutritional diffusion, but also cellular proliferation and invasion of the scaffold [2].

Therefore, the field of TERM often relies on the use of additive manufacturing methods, often referred to as 3D printing. Most commonly, optical fabrication techniques based on 1-photon absorption are chosen, with stereolithography (SLA) being the most popular. SLA produces 3D objects in a layer-by-layer procedure by selectively curing a photosensitive resin. Freedom of design and a high

degree of porosity are two highly-valued benefits which have propelled SLA in the field of TERM, this method is however limited to a feature resolution of around 20 μm [3].

This, in turn, imposes a lower thickness limit on the struts separating the pores, which in turn, restricts the overall volumetric porosity of a scaffold (i.e. pores can only be spaced so close to each other). Other methods, such as electrospinning, allow the fabrication of scaffolds with higher porosity of up to 97%. However, the tight packing of fibers on the micrometer scale has been reported to impede the process of cellularization [4, 5]. While melt electrowriting allows the controlled stacking of thin fibers, this method cannot accurately reproduce intricate 3D structures based on CAD models, the same way photopolymerization-based techniques, such as SLA and two-photon polymerization (2PP) can.

2PP is a high-resolution 3D printing method, allowing to obtain volumetric elements of submicrometer resolution. Compared to SLA, 2PP permits to fabricate structures with a significantly higher spatial resolution. 2PP requires the combined energy of two photons to initiate photopolymerization, which in turn confines the phenomenon to the focal plane of the laser beam. This way, a high-resolution freeform 3D structures can be patterned into the resin by only moving the focal point of the laser [6].

Compared to other techniques, only a small number of biodegradable scaffolds have been reported with 2PP, even though it is a highly applicable technique. A major drawback to 2PP is that the increase of resolution is linked to comparatively low throughput. At laser writing speeds as low as 0.1 mm s^{-1}, which are not uncommon, the production of a cube of 1 cm^3 was estimated to take 300 years by Stichel *et al* [1] Even though faster speeds have been reported [7], scaffolds produced with 2PP are usually rather small to keep within a reasonable production time limit. So far, the largest reported scaffold had a side length of 5 mm, which underlines why 2PP faces a substantial acceptance barrier for TERM applications [1].

A further limiting factor for the scaffold production with 2PP is the availability of materials. Compared to other fabrication techniques, the number of reported biodegradable scaffolds produced with 2PP is very low. A possible reason for this is the lack of biodegradable and commercially available photopolymers suitable for 2PP. A point in favor of the development of more biodegradable resins is that the nonlinear absorption makes the resin preparation far less complex by not requiring additional light absorbers (e.g. orasol orange or titanium dioxide particles) [8]. The absence thereof further reduces the risk of toxicity of the final scaffold.

Polymers typically processed with SLA provide an excellent starting point for the use with 2PP. Typically, (meth-)acrylated poly(ester) polymers are used for SLA. As such, polylactic acid (PLA) has found use in both, SLA [9] and 2PP [10], for a range of applications, such as bone tissue formation. Another polymer, previously used for SLA, is poly(trimethylene-carbonate) (PTMC). Due to its peculiar degradation mechanism (surface erosion driven by enzymatic erosion), PTMC has shown to be a highly suitable polymer for the fabrication of scaffolds for bone tissue engineering and hence poses a great potential for the use in 2PP [11].

With all the recent developments in 2PP for TERM applications, some technical limitations remain. Currently, large scaffolds require a long time to produce and stitching adjacent field of views will leave a noticeable transition. Moreover, the limited availability of biocompatible and biodegradable photopolymers and suitable photoinitiators, as well as the high price point of 2PP systems is inhibiting the fast adoption of the technique for TERM applications.

In this work, we mitigate some of the mentioned bottlenecks of 2PP. First, we detail the composition of a highly photoreactive resin based on PTMC. Through a systematic screening study of process parameters for 2PP, we further show the production of novel biocompatible and biodegradable scaffolds with an unprecedented large size. The structures have a high volumetric porosity of 96% and complex microarchitectures. Moreover, these scaffolds proved excellent cellular invasion and differentiation. This shows the suitability of 2PP as an additive manufacturing technique to produce high-resolution scaffolds with highly relevant properties for TERM.

2. Materials and methods

2.1. Photopolymer synthesis

3-armed PTMC, was synthesized by ring-opening polymerization (ROP) of trimethylene carbonate (TMC) in a three-necked round-bottomed flask with trimethylolpropane (initiator) under argon atmosphere at 130 °C for 3 d (50 g (0.49 mol) TMC and 1.48 g (5.0 mmol) trimethylolpropane with 0.065 g of $Sn(Oct)_2$ as catalyst). The 3-armed PTMC (PTMC oligomer) was dissolved in dichloromethane after cooling to room temperature. Methacrylate-functionalized PTMC (PTMC-MA macromer) was synthesized by the following method. Under argon, 0.05 g hydroquinone, 10 ml triethylamine (0.072 mol) and 12 ml methacrylic anhydride (0.081 mol) were added. The mixed solution was reacted with stirring for 5 d in the dark at room temperature. The solution was precipitated and washed in cold methanol to remove unreacted monomer and other compounds. The PTMC-MA containing methanol was firstly dried in the dark at ambient conditions overnight and then dried in vacuum for another 7 d at room temperature (the synthesis route is shown in SD 1). The PTMC oligomer and the PTMC-MA macromer were analyzed by ^{1}H-NMR (Bruker Ascend 400/Avance III

400 MHz NMR spectrometer) to determine the average molecular mass (Mn) and the degree of functionalization of PTMC-MA. We obtained PTMC of 4300 g mol^{-1} with a degree of methacrylation for the PTMC-MA of 97%.

2.2. Resin preparation

PTMC resin was prepared by dissolving 3-armed PTMC-MA in tetrahydrofuran (THF) with 0.5 wt% M2CMK as a photoinitiator, providing a two-photon absorption cross section of around 100 Göppert-Mayer (GM) units [13]. After 24 h, the resin was heated to 150 °C to evaporate the THF. To eliminate air bubbles, the resin was placed in a vacuum for 10 min before dispensing into appropriate sample holders. The sample holders consisted of a 3 mm thick aluminum sheet the size of a microscope slide with holes, sealed on one side with cover slips using 2-component glue. Before printing with 2PP, the PTMC resin was heated to 50 °C.

2.3. Laser setup, 2PP printing and post-processing steps

A tunable femtosecond-pulsed laser (MaiTai eHP DeepSee, Spectra-Physics) was operated at 800 nm at a repetition rate of 80 MHz and a pulse duration of 70 fs after the microscope objective (UPlanS-Apo, 10x/0.4 NA, Olympus, Japan). Laser positioning was done by a dual-axis galvanometric scanner (Scanlabs, Germany) and sample positioning was done by a microscope stage (ScanPLUS IM, 120 × 180, Märzhäuser-Wetzlar, Germany). A writing speed of 1 000 mm s^{-1} was used and different laser intensities were screened from 20 to 380 mW. The schematics of the process is shown in figure 1. The laser was focused through a cover slip into the material. Due to the resin's inherent viscosity, the structures were printed top-down. Hence, the already polymerized part never obstructed the laser beam.

The buckyball structures were designed in SolidWorks (Dassault Systèmes, France). After structuring with 2PP, the sample holder was submerged in THF for 1 h to dissolve any uncrosslinked PTMC-MA. Two additional THF washing steps were carried out before storing the scaffold in 1-propanol.

2.4. Scaffold characterization

Optical analysis of the produced scaffolds was performed with a confocal microscope (LSM700, Zeiss, Germany), a scanning electron microscope (SEM, Philips XL Series 30) and and high resolution micro computed tomography (μCT). μCT was performed on a Scanco 50 scanner (Scanco Medical AG, Switzerland) at 70 kV, 57 μA with an 0.5 mm Al filter at 1000 ms integration time and 1500 Projections. Subsequently, the scaffold was skeletonized and strut elements were segmented by removing the intersecting nodes. Local strut thickness was measured and graphically overlayed as a representative sphere of corresponding diameter at the center of each strut for better visualization.

2.5. Cell seeding and culture conditions

Prior to cell seeding, the scaffolds were sterilized in 70% ethanol and incubated in DMEM with 10% (v/v) FBS for 24 h. Immortalized human adipose-derived mesenchymal stem cells (hASC/hTERT) (Evercyte, Austria) were expanded using EGM™-2 BulletKit™ medium (Lonza, Switzerland) supplemented with 10% (v/v) newborn calf serum (NBCS) (Gibco, New Zealand) and maintained at standard culturing conditions (37 °C, 5% CO_2, humidified atmosphere). Ten microliters of hASCs suspension (containing 125 000 cells, passage 8) were seeded on top of each scaffold in agarose-coated 24-well plates. Cell-seeded scaffolds were then transferred to either control medium (composed of high glucose Dulbecco's modified Eagle medium [HG-DMEM; Gibco, United Kingdom] supplemented with 10% NBCS and 1% penicillin-streptomycin), chondrogenic medium (CM) or osteogenic medium (OM). CM consisted of HG-DMEM supplemented with 1% insulin–transferrin–selenium supplement (Gibco, United Kingdom), 1% of P/S, 1% 1 M HEPES buffer (Mediatech, VA), 0.1 mg ml^{-1} sodium pyruvate, 50 μg ml^{-1} L-proline, 50 μg ml^{-1} ascorbic acid 2-phosphate, 100 nM dexamethasone, and 10 ng ml^{-1} of human transforming growth factor β_3 (Peprotech, NY) and human bone morphogenic protein 6 (R&D, MN). OM was composed of HG-DMEM supplemented with 10% (v/v) NBCS, 4 mM L-glutamine, 1% (v/v) P/S, 10 nM dexamethasone, 150 μM ascorbic acid 2-phosphate, 10 mM β-glycerophosphate, and 10 nM 1,25-vitamin D3. The medium was changed three times a week for 28 d.

2.6. Cell viability

Viability of the cells was determined using a Live/Dead® assay (Invitrogen, OR) using 0.2 μM calcein-AM (live stain) and 0.6 μM propidium iodide (dead stain) in serum-free medium for 60 min at 37 °C. The viability of the cells was monitored on day 14 and day 28 using a confocal laser scanning microscope LSM 700 (Zeiss, Germany).

2.7. Scanning electron microscopy (SEM)

SEM analysis of the constructs was performed after fixation in buffered paraformaldehyde at 4%, followed by gradual dehydration in ethanol and by immersion in hexamethyldisilazane (Sigma-Aldrich). After drying, the samples were sputter-coated with Au and investigated by SEM.

2.8. Histology

After 28 d of cultivation, cell-seeded scaffolds were washed in PBS and fixed overnight in

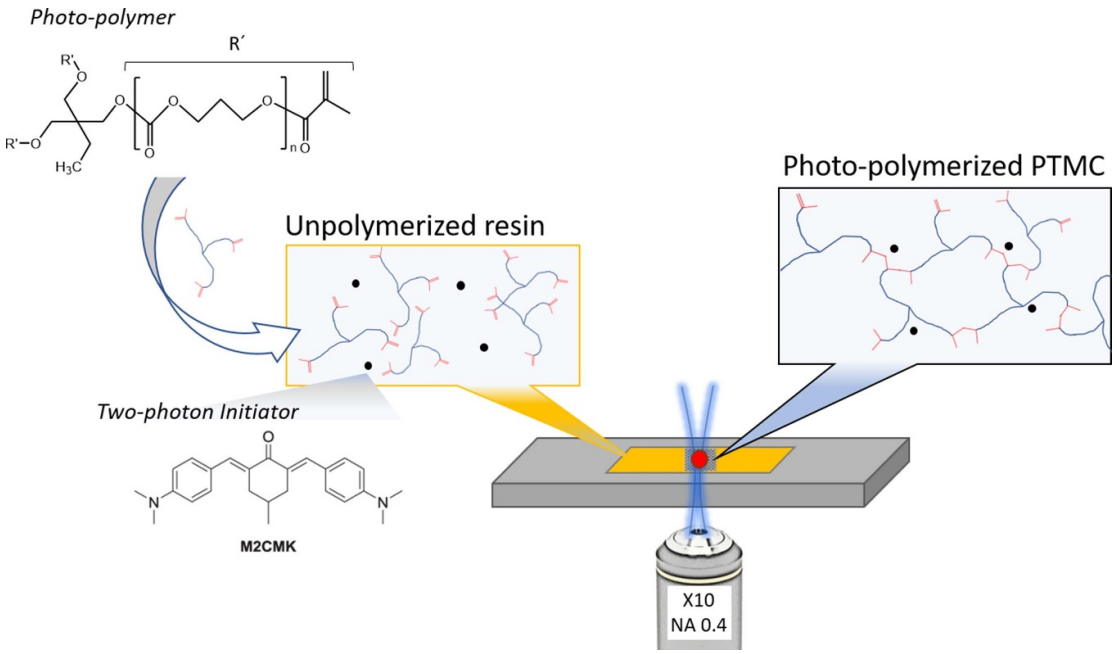

Figure 1. Schematics of 2PP processing. A thick layer of resin based on PTMC-MA and M2CMK is casted into the sample holder. Scaffolds are then produced via 2PP within the volume of the resin through photo-crosslinking of the methacrylate groups of the PTMC-MA.

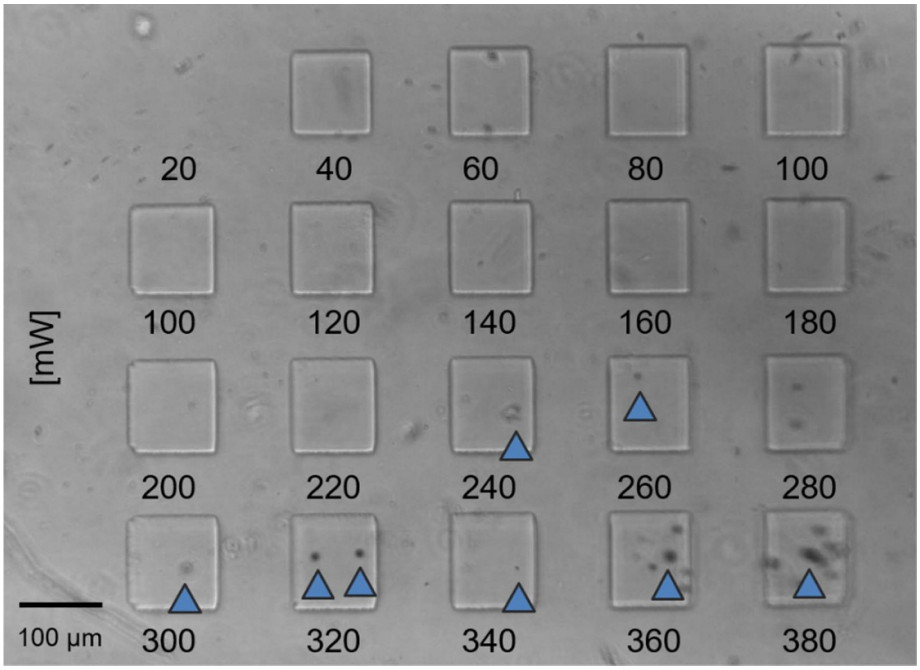

Figure 2. Optimization of two-photon polymerization (2PP) threshold for the PTMC-MA based resin. Microscopic visualization of cubes (100 × 100 μm) printed using 2PP with increasing power intensities from 20 to 380 mW. The occurrence of bubbles inside the PTMC-MA due to thermal effects is denoted with the blue triangles.

Roti®Histofix 4% (Carl Roth, Germany) at 4 °C. Samples were embedded in paraffin blocks and processed at the Histopathology Department (Vienna BioCenter Core Facilities GmbH, Austria) for Hematoxylin-Eosin (H&E), Von Kossa, Alcian Blue staining, and for proliferative marker Ki67 immunostaining.

2.9. Biochemical assays

At different time points, samples were washed and digested with 125 μg ml^{-1} papain in 0.1 M sodium acetate, 10 mM L-cysteine-HCl, 50 mM EDTA (all from Sigma-Aldrich) adjusted pH 6.0 and incubated at 55 °C under constant shaking for 18 h (n = 3 for each group). DNA content of each

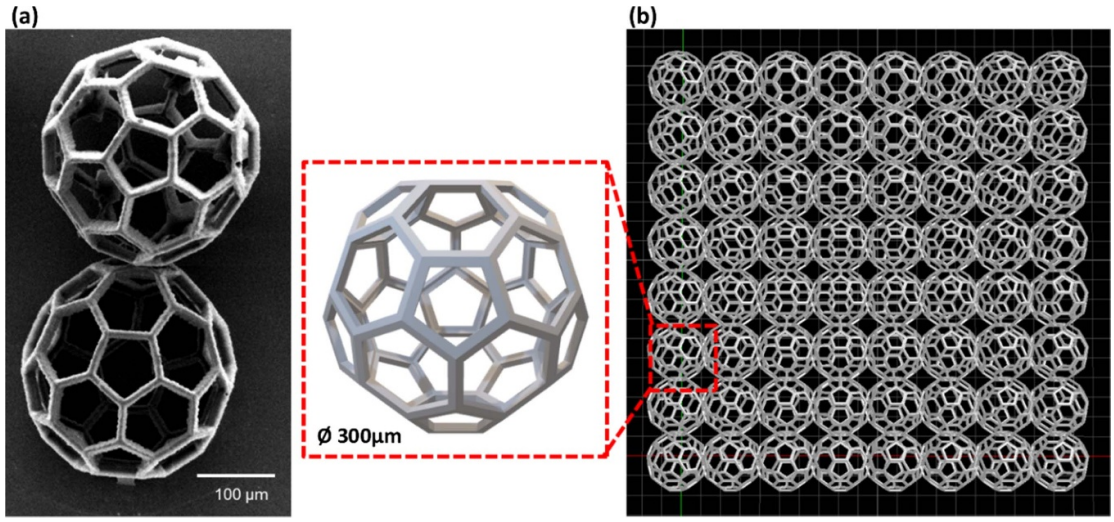

Figure 3. Design of buckyball-based scaffold. (a) SEM picture of 2 BB units printed at optimized parameters (b) 3D render of the scaffold consisting of an 8 × 8 × 3 array (l, w, h) of BB units with a diameter of 300 μm each. The final size is 2.4 × 2.4 × 0.9 mm (l, w, h).

sample was quantified using the Quant-iT PicoGreen assay (Thermofisher). The content of sulfated glycosaminoglycans (sGAG) was quantified using the dimethylmethylene blue dye-binding assay (DMMB, Blyscan, Biocolor Ltd., United Kingdom), with a chondroitin sulphate standard.

3. Results

3.1. Optimization of PTMC-MA printing using 2PP

In order to define an optimal 2PP processing window for the PTMC-MA, a laser intensity screening test was conducted. For this test, a fixed laser writing speed of 1000 mm s^{-1} was selected and an assay with a stepwise increase of the laser power from 20 to 380 mW was performed. The results presented in figure 2 revealed the 2PP processing window between 40 to 220 mW. Below and above this threshold, either no polymerization occurred or material degradation was visible, respectively. The first is seen by the absence of a printed structure at a laser intensity of 20 mW, whereas the latter was seen through the occurrence of bubbles due to thermal effects. The test cubes were printed at a fixed hatch value of 0.5 μm and a fixed dZ value of 1 μm, which describe the distance of two adjacent laser lines in *xy*- and *z*-direction, respectively. Consequently, the 2PP processing window was further optimized in a subsequent step to find optimal printing values for hatch and dZ. These values directly influence the quality of the printed parts and are important when printing more intricate structures, such as the architecture of the macroscaffolds. Therefore, we produced 3D microstructures consisting of hexagons and pentagons arranged to form a low-polygon sphere based on the fullerene structure. The microstructures, also referred to as buckyballs (BB) [12] were produced at varying hatch and dZ values ranging from 0.4 μm to 1.5 μm and at 100, 130 and 160 mW. The so obtained parametrically arrayed structures were then microscopically assessed whether they match their 3D model in terms of strut thickness and open pores.

We concluded that a laser intensity of 130 mW, a hatch value of 0.8 μm and a dZ value of 1 μm would yield structures that best resemble their 3D model. Using these parameters, printing of a single buckyball took around 20 s, which was considered reasonable for our application.

The 2PP fabrication of a single BB is shown in SD 2 (printing sped up 10 times, with a bottom-up view). After dissolution of unpolymerized materials in THF and drying in HMDS, the BBs were characterized using SEM (figure 3(a)). The measured diameter of the buckyball was around 300 μm with a strut width of around 20 μm and strut thickness of around 30 μm. The measured values correspond to the dimensions of the 3D model indicating that the printing parameters were chosen correctly.

Once the processing parameters of the PTMC-based resin were established, a porous scaffold was fabricated. The scaffold consisted of an array of 8 × 8 × 3 interconnected buckyballs forming a rectangular and highly porous structure (figure 3(b)). It had a side length of 2.4 mm, a height of 0.9 mm and took around 60 min to produce (figures 4(a)–(c)). The structure was designed to feature a high volumetric porosity to support rapid cell invasion and nutrient exchange. SEM imaging confirmed that the delicate structures were preserved during post-processing of the sample.

In a last step, we further upscaled the scaffold to a side length of 18 × 18 × 0.9 mm (l, w, h), which, to the best of our knowledge, is the largest biodegradable

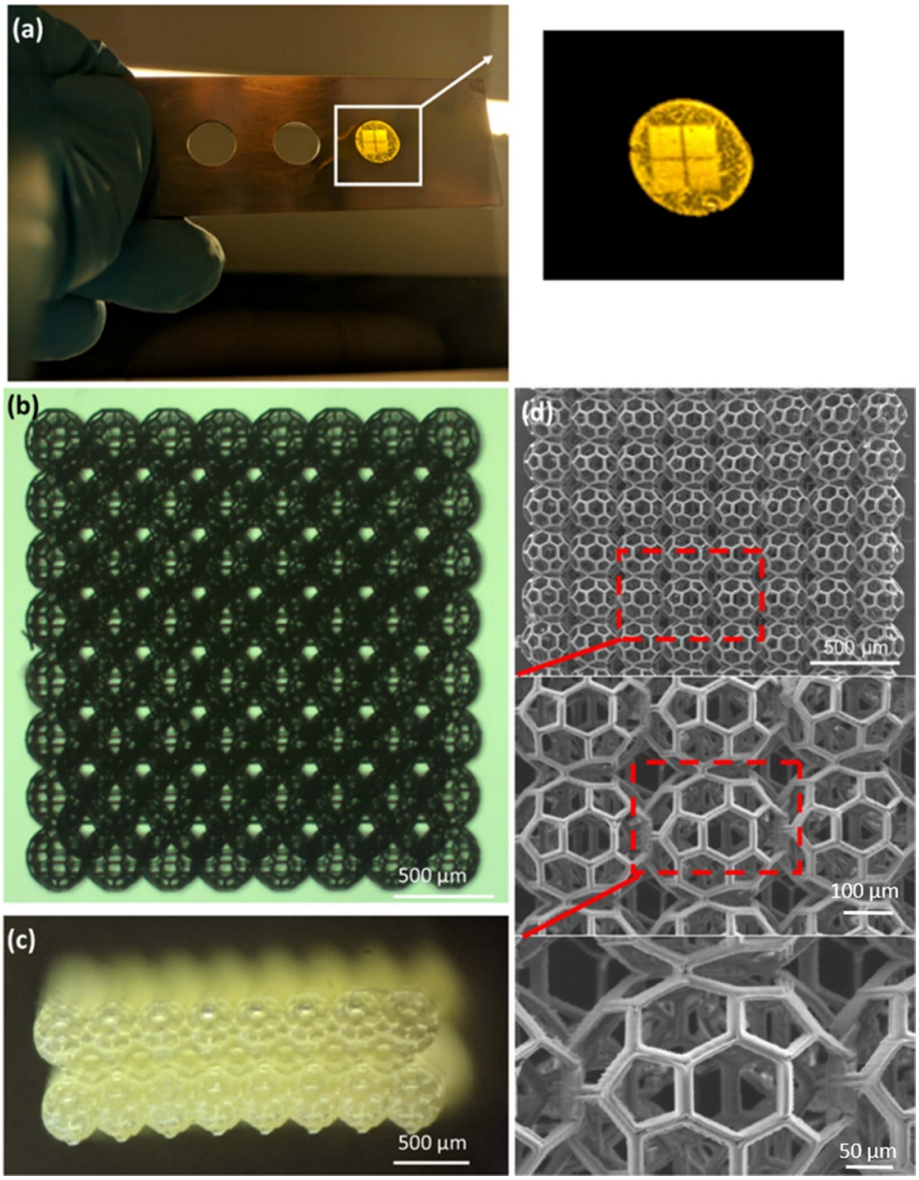

Figure 4. Scaffolds produced with 2PP (a) Illustration of the sample holder used for 2PP structuring containing 4 scaffolds still embedded in the unpolymerized resin. Macroscopic (b) top view and (c) side view of the tri-layered PTMC-based scaffold. (d) SEM images of the scaffold at various magnifications (x50, x150 and x300).

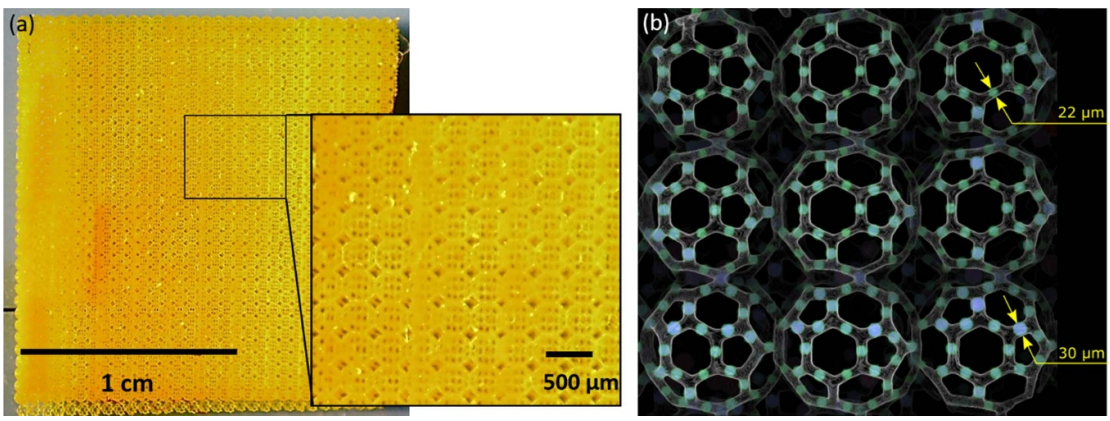

Figure 5. Upscaled scaffold printed using 2PP (a) Macroscopic observation of the large 2PP printed scaffold with a side length of 18 mm (b) Micro-computed tomography with overlaid spheres visualizing the local strut thickness.

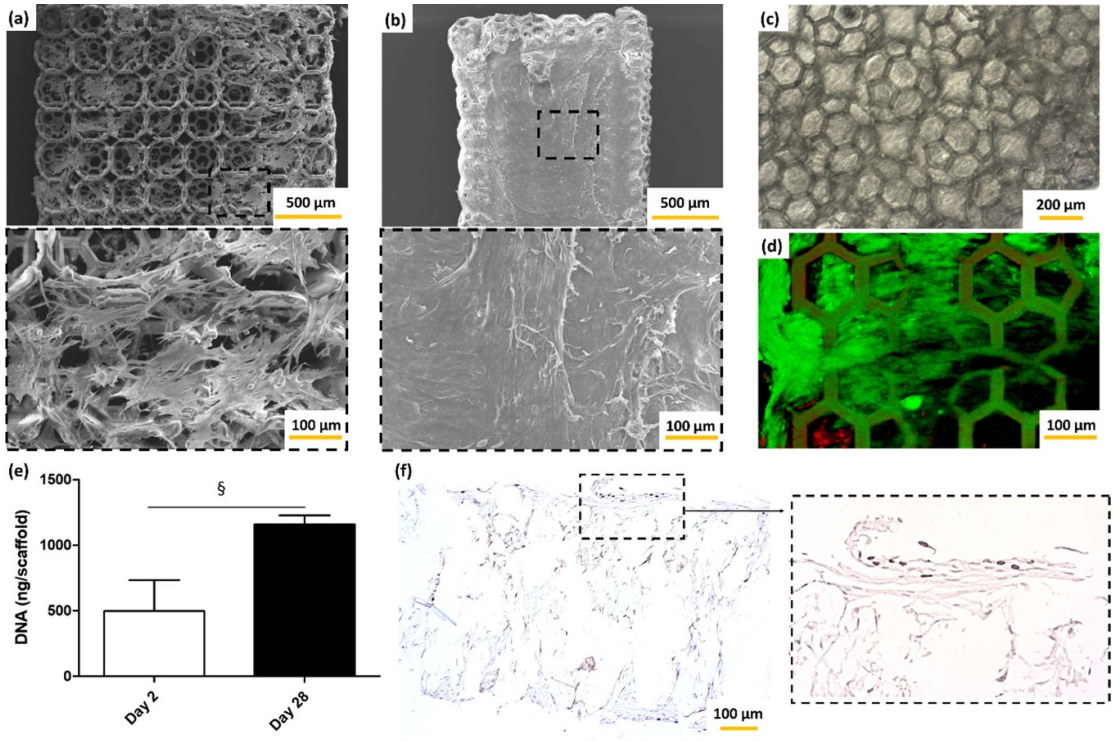

Figure 6. 2PP-produced PTMC-MA scaffolds support cell invasion and proliferation. SEM images of cell-seeded scaffolds day 2 (a) and day 28 (b) post seeding. (c) Bright field and (d) Live/Dead illustrations of the colonized scaffold at day 28. (e) Cellular proliferation quantified by DNA assay (§ indicates statistical significance) and (f) Ki67 immunostaining (nuclei of positive proliferative cells are stained in black).

scaffold produced using 2PP to date (figure 5(a)). It is composed of 3072 BB units, took 16 h to print and shows the potential of 2PP to produce highly-intricate scaffolds for TERM.

The scaffold was imaged using high-resolution micro-computed tomography, which showed its structural integrity (SD 3) and revealed a strut thickness ranging from 22 to 30 μm with a median thickness of 25 μm (figure 5(b)).

3.2. 2PP-produced PTMC-MA scaffolds support stem cells proliferation and differentiation

Scaffolds printed from PTMC-MA using 2PP supported the adhesion and proliferation of hASCs. Two days post-seeding, hASCs attached to the scaffold and exhibited elongated filopodia (figure 6(a)). Over 28 d of culture, the hASCs colonized the entire scaffold and formed a dense cellular layer on the surface of the scaffold (figures 6(b) and (c)). Live/dead staining conducted at day 28 showed a high cellular viability (figure 6(d)). The proliferation of the hASCs was validated by the significant increase of DNA (figure 6(e)) and presence of ki67-positive cells (figure 6(f)). We then evaluated whether PTMC-MA scaffolds would support hASCs to differentiate towards chondrogenic and osteogenic phenotypes.

When cultivated in appropriate media, the seeded macroscaffolds supported hASCs chondrogenic and osteogenic differentiation. SEM cross section demonstrated that such 3D scaffolds, due to their high degree of porosity, were easily colonized by the cells (figure 7(a)). sGAG secreted by the hASCs seeded on the scaffolds was shown to be significantly higher for CM condition compared to control condition (figure 7(b)), which was also shown by the positive Alcian Blue staining (figure 7(c)). SEM and histology sections demonstrated that a large amount of ECM was deposited throughout the thickness of the structures. Finally, once cultivated in osteogenic condition, hASCs were able to differentiate toward osteoblasts and to deposit calcium precipitates as shown by the positive Von Kossa staining (figure 7(d)).

4. Discussion

4.1. 2PP is a relevant technique to print TERM scaffolds

SLA and digital light processing (DLP) are the most used lithography-based additive manufacturing processes for the production of scaffolds for TERM. They enable the rapid production of scaffolds of clinically-relevant sizes and porosities while also enabling rapid design iterations.

However, their minimal resolution is dictated by the diameter of the laser beam [26]. In contrast, printing processes based on two-photon absorption permit to achieve a significantly higher resolution, albeit at the expense of the printing time, which typically affects a scaffold's final size.

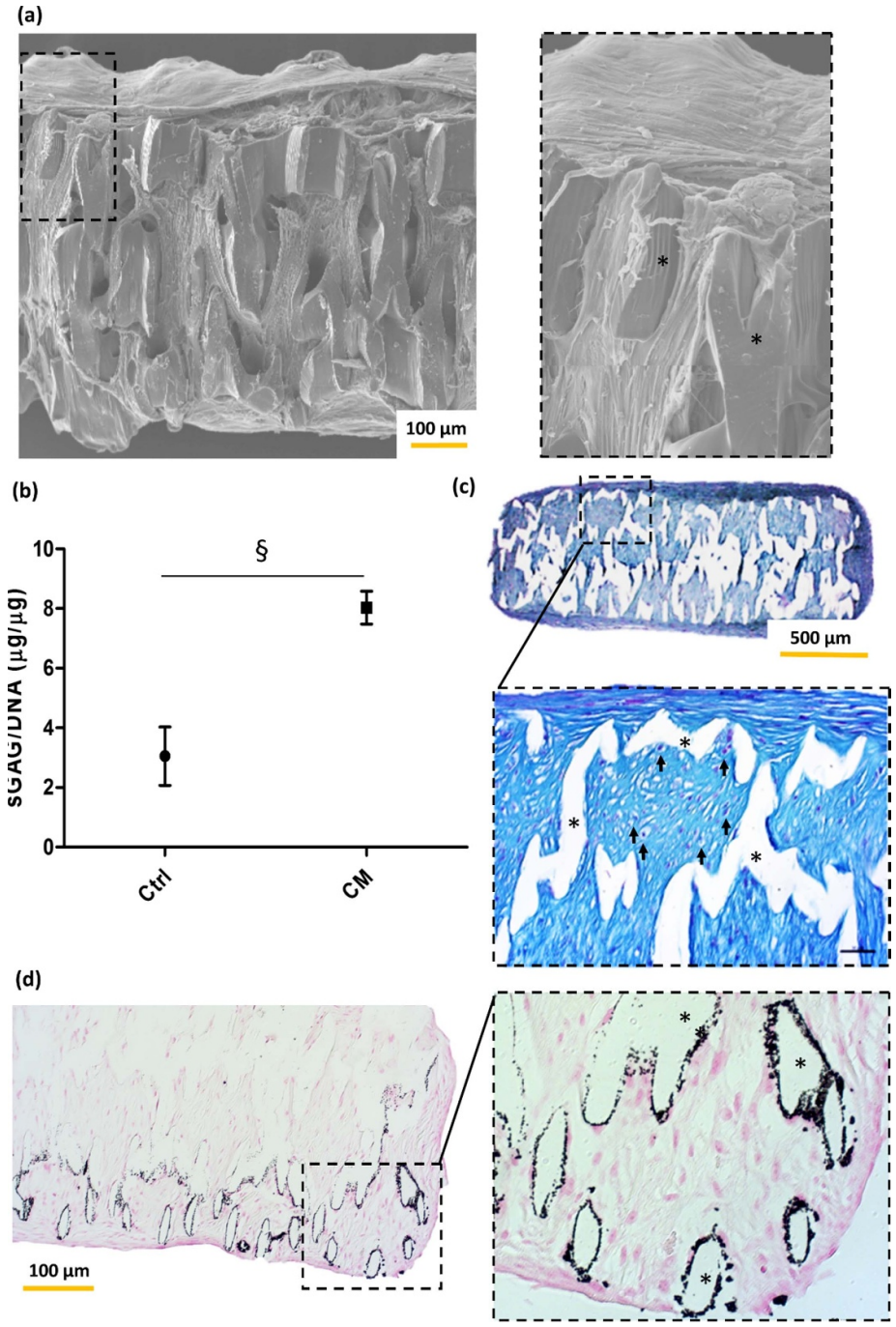

Figure 7. PTMC-MA scaffolds printed using 2PP support differentiation of hASCs. (a) SEM cross-section of the scaffold after 28 d of incubation in chondrogenic medium (CM). (b) Quantification of sGAG secretion by hASCs (§ indicates significance) in control medium versus CM and (c) histological staining of sGAGs using Alcian Blue at day 28. Black arrows show the chondrocytes embedded in the secreted ECM. (d) Von Kossa staining showing in black the calcium mineralization after 28 d of hASCs cultivation in OM. Cross-sections of the scaffold are marked with black asterisks.

This relation is further reflected in the available literature on scaffolds produced with 2PP for TERM.

While most of the available reports demonstrate a high resolution, the largest construct to date, to the best of our knowledge, featured a side length of only 5 mm (figure 8). Despite being highly porous (∼80%), this construct took nevertheless 4 h and 20 min to print and was produced from Ormocer®, a commercial, non-biodegradable hybrid polymer [1].

In our work, we demonstrated that we were able to significantly increase the volume by almost an order of magnitude by producing scaffolds with a side length of 18 mm and a volume of 292 mm^3.

On the hardware side, this was made possible by using a low magnification objective (x10, numerical aperture of 0.4) and a fast writing speed (1000 mm s^{-1}), whereas optimizing the material-specific parameters and the printing settings was critical on the software side. Together, this

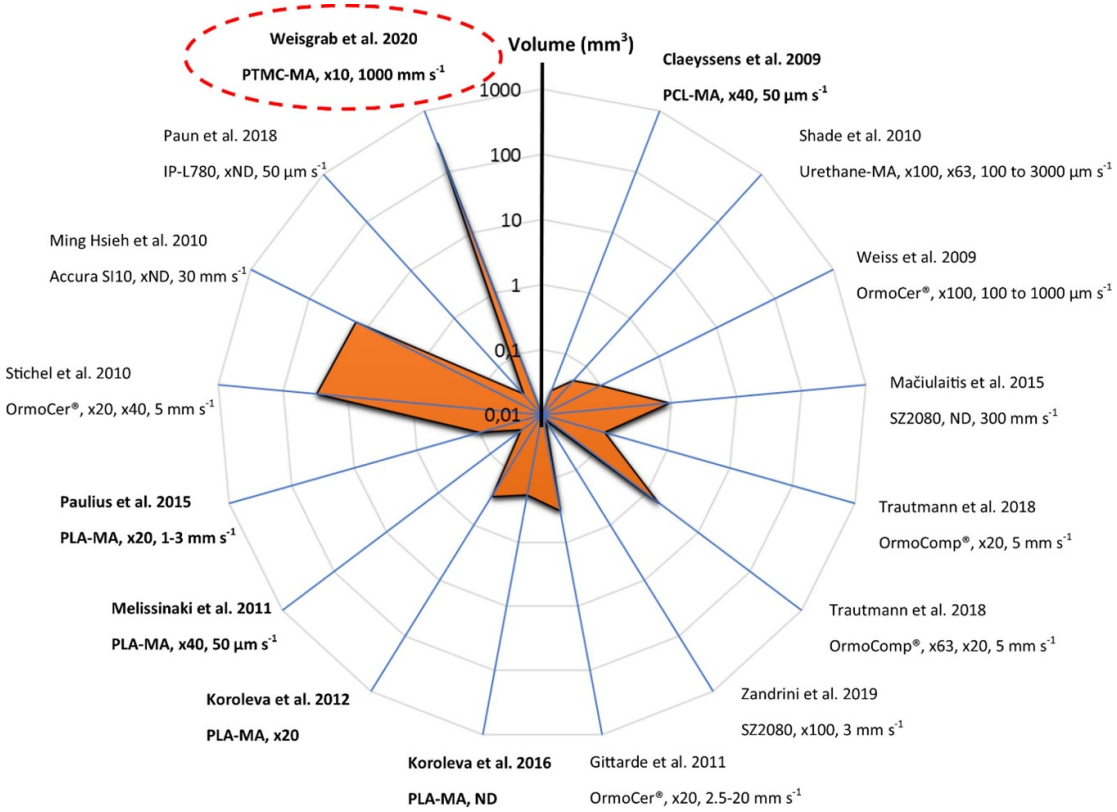

Figure 8. Our work introduces a 2PP printed scaffold, novel not only regarding its composition, but also its unprecedented large size. Graphical representation of the volumes of scaffolds printed with 2PP presented in the literature, with the nature of the photopolymer, the objective used and the writing speed. ND indicates that either the microscope objective or the writing speed is not described in the experimental section of the reference. References using biodegradable biomaterials are highlighted in bold characters. List of the references is available here [1, 7, 14–25].

enabled the fast writing speeds of 1 h for the smaller scaffold presented in figure 4 and 16 h for the larger scaffold presented in figure 5.

Achieving fast printing speeds is one the key factors to realizing constructs with a relevant size for TERM. In previous publications, printing speeds ranged from 5 mm s^{-1} [1, 18] up to 30 mm s^{-1} [7]. However, writing as slow as 0.1 mm s^{-1} is not uncommon and at these speeds, the production of a 1 cm^3 block was estimated to take 300 years by Stichel *et al* [1]

Working at fast writing speeds requires photoinitiators with a high two-photon absorption cross section (δ). Photoinitiators typically used in 1-photon absorption, such as different types of Irgacure have δ values in the order of around 20–30 Göppert Mayer (GM) units [27]. Photoinitiators that were specifically developed for two-photon absorption, such as M2CMK used in this work, have a δ value of around 150 GM, requiring a lower laser intensity for initiation [13]. This, in turn, allows faster writing speeds but also a lower initiator concentration, which is favorable for the design of biocompatible scaffolds. Lastly, the absorption maximum of the chosen photoinitiator is of importance, as light in the near infrared has a higher penetration depth than UV-light [14].

Apart from material properties and print settings, technical advances of the 2PP setup are also of importance. For instance, Trautmann *et al* developed a single-line single-pass process to increase the speed of scaffold fabrication [18]. This strategy takes advantage of true 3D writing and does not follow a layer-by-layer approach, enabling the fabrication of scaffolds with a surface larger than 9 mm^2 and a 140 times faster throughput. The major downside of this technique is the approximation of cubic structures by inlaying ellipses, as it lowers the accuracy and limits the type of structures that can be printed.

A different approach to upscaling 2PP production is the employment of multiple foci. By splitting the beam before the scanner, the foci can be moved in parallel. Using a spatial light modulator, a 16-foci system was demonstrated to produce a scaffold with a surface of 1.6 mm^2 tested with bovine endothelial cells [20]. Using the same approach, a 2- and 6-foci setup was shown for the fabrication of nichoids for stem cell expansion [28]. Parallel foci further require a higher laser output power, which may result in laser drifting over time and possibly thermal damage of the crystal screen. Another disadvantage of multiple foci is the requirement to lower the scanning speed which impacted the time gain significantly [20, 29]. Zandrini *et al* showed the polymerization of SZ2080

resin with a laser energy of 260 mW and a translation speed of 3 mm s^{-1}. In comparison, our scaffold was written at 1 000 mm s^{-1} using half the laser intensity, which consequently increased our volumetric processing time by a factor of 166 and 55 compared to the 2- and 6-foci setup, respectively. The combination of fast writing speeds, a highly reactive photoinitiator and optimized process parameters have resulted in a scaffold for TERM applications with a previously unreported volume.

With regards to the microarchitecture of the scaffold, we aimed at producing a structure with a small pore size and high volumetric porosity at reasonable production times. Porosity is essential to create a microenvironment favorable for the cell proliferation, ECM deposition and suitable neo-tissue formation. While a high porosity (>90%) is generally regarded beneficial for osteogenic scaffolds [19, 30] there has been a wide range of reported pore sizes (50–500 μm) suitable for osseous tissue further depending on what type of bone is mimicked [30–32]. Numerous publications have shown that osteogenesis is more favorable in scaffolds with pores around 300 μm and larger [30, 33–37]. Naturally, other factors, such as pore geometry, scaffold material, cell type, cell culture conditions and surface topology also play an important role in deciding a cell's fate.

In finding a compromise between these key parameters, we have created a scaffold with a side length of 18 mm with pore sizes of 300 μm and a volumetric porosity of 96% in around 16 h. Choosing such a highly-porous structure with narrow pore sizes, only leaves space for small scaffold struts. This stringent criterium highlights the need for 2PP as an appropriate fabrication technique for TERM, as many conventional photofabrication techniques based on 1-photon absorption would fall short of this task. Moreover, the increase in resolution provided by 2PP could further allow the addition of micro-patterns on a scaffold's surface to further accelerate the cellular fate towards osteogenesis [38].

4.2. Novel biocompatible PTMC-based resin for 2PP

The material shown in this work is another point of novelty and of high importance. As shown in figure 8, scaffolds produced by 2PP are usually composed of commercial resins, such as Ormocer®, OrmoComp® or SZ2080. While these were shown to be cytocompatible, they are not biodegradable [15, 39, 40]. In general, biocompatible and biodegradable materials are preferred for implantation, as they do not create potentially toxic by-products during degradation. Although there have been efforts to make commercially available and biodegradable materials, as seen with bioORMOCER®, to the best of our knowledge, this material has not been demonstrated with 2PP.

More recently, reports on scaffolds produced from photopolymerizable polyesters, such as PLA and PCL have emerged. Interestingly, these materials were also shown to be polymerizable using 2PP after being functionalized by methacrylate moieties [10, 17]. As an alternative to these polyesters, we introduced the photopolymerizable PTMC-MA. Grijpma *et al* have previously shown that this polymer can be processed with SLA to form scaffolds for numerous applications, such bone [41], vascular [42] or even meniscus repair [43]. To the best of our knowledge, this polycarbonate-based photopolymer has not been processed with 2PP yet. Due to its short size of only 4.3 kDa and the presence of the three MA-branches, the methacrylate double bond conversion and hence the crosslinking polymerization is statistically more efficient compared to longer and linear macromers. This is beneficial for the production of large scaffolds, as the resin can be processed with a fast writing speed and with a high laser power without burning the biomaterial (130 mW at 1000 mm s^{-1}). In comparison, PLA-MA was processed with a writing speed of 1 to 3 mm s^{-1} at 15 mW [20] and with 50 μm s^{-1} at 30 mW [44].

The cytocompatibility study in this work showed great cellular acceptance of the PTMC-based scaffolds produced with 2PP. These results are in accordance with the observations by Guillaume *et al* on PTMC scaffolds produced by SLA, suggesting that 2PP has no adverse effect on the scaffold production [41, 45]. Nevertheless, the main difference between the two structures is the higher porosity (*i.e.* 96%) that was reached with 2PP when compared to structures with a porosity of around 70% printed using SLA. 2PP allows the production of scaffolds with a very low material density while still providing substantial surface contact to encourage physical cell adhesion and proliferation. This permits a fast cell invasion and penetration and, in turn, results in a high ECM deposition. After seeding the scaffold with hASCs and cultivating them in chondrogenic conditions, homogenous sGAG distribution could be seen throughout the scaffold. Moreover, hASCs differentiated towards osteoblasts as demonstrated by the presence of calcium phosphate (CaP) mineralization. Contrary to the sGAG deposition, CaP precipitation was not observed uniformly throughout the cross section of the scaffold but was localized at the interface between scaffold struts and ECM. This is not an isolated finding as tissue mineralization is commonly seen to initiate at the interface with the implant [46, 47]. Further tailoring the surface properties of the scaffold to provide CaP nucleation sites would help in increasing the scaffold's osteogenic potential. For instance, Werner *et al* have demonstrated that surface curvature impacts the fate of stem

cell differentiation, with convex surfaces promoting osteogenesis [48]. Further, the inclusion of micro-patterns on the scaffold surface has previously shown to impact cell-adhesion and differentiation of pre-osteoblast cells [38]. Such 3D geometric cues could easily be integrated in the 2PP manufacturing workflow of implants dedicated to bone regeneration.

Previous literature has shown cell acceptance of scaffolds produced with 2PP, but to the best of our knowledge, cell penetration, scaffold invasion and ECM production at this scale have never been reported.

Lastly, as mentioned in the introduction, this research represents a first proof-of-concept that 2PP can produce highly intricate structures of large-scale sizes with excellent cytocompatibility when optimal printing parameters are chosen. In the future, we plan to replace the repetitive subunits in this scaffold with similarly intricate structures that result in a more anisotropic architecture and hence better resemble the conditions found in most tissues. The opportunity offered now by 2PP has been the holy grail for many researchers questing to recreate artificial scaffolds biomimicking for instance the anisotropic architecture of osteochondral tissues, amongst others [49, 50].

5. Conclusion

Due to the non-linear absorption of 2PP, a range of structures with highly complex architectures have been presented over the last decade. This high degree of detail is usually connected to a long printing time and therefore scaffolds are only produced at a small scale. To become a relevant technique for the production of TERM scaffolds, the constructs must be significantly scaled up while being printed in a shorter time. Here, we demonstrated that by: (i) formulating a specialized photosensitive resin, based on a highly-reactive three-armed methacrylated PTMC with a photoinitiator specifically developed for 2-photon absorption, and by (ii) optimizing the 2PP printing parameters, large structures were produced at an unprecedented speed of 1000 mm s^{-1}. The resulting constructs have a volume of an order of magnitude higher than previously reported constructs and have proven to be suitable for homogenous cell invasion and matrix deposition. This research showed advancements in two areas for 2PP, namely the processing of a new biomaterial and the production of highly porous and biodegradable scaffolds at a relevant scale for TERM.

Acknowledgments

This project has received funding from the European Research Council (ERC) under the European Union's Horizon 2020 research and innovation programme (Grant agreement No. 772464).

ORCID iDs

Gregor Weisgrab https://orcid.org/0000-0003-4856-2208
Olivier Guillaume https://orcid.org/0000-0003-0735-113X
Dirk Grijpma https://orcid.org/0000-0002-2678-2480
Aleksandr Ovsianikov https://orcid.org/0000-0001-5846-0198

References

[1] Stichel T 2010 Two-photon polymerization as method for the fabrication of large scale biomedical scaffold applications *J. Laser Micro./Nanoeng.* **5** 209–12
[2] Hollister S J 2005 Porous scaffold design for tissue engineering *Nat. Mater.* **4** 518–24
[3] Melchels F P W, Feijen J and Grijpma D W 2010 A review on stereolithography and its applications in biomedical engineering *Biomaterials* **31** 6121–30
[4] Sisson K, Zhang C, Farach-Carson M C, Chase D B and Rabolt J F 2010 Fiber diameters control osteoblastic cell migration and differentiation in electrospun gelatin *J. Biomed. Mater. Res.* A **15** 1312–20
[5] Lee J, Cuddihy M J and Kotov N A 2008 Three-dimensional cell culture matrices: state of the art *Tissue Eng.* B **14** 61–86
[6] Stampfl J, Liska R, Ovsianikov A*et al* 2016 *Multiphoton Lithography* J Stampfl, R Liska and A Ovsianikov eds (Weinheim: Wiley-VCH Verlag GmbH & Co. KGaA)
[7] Hsieh T M, Benjamin Ng C W, Narayanan K, Wan A C A and Ying J Y 2010 Three-dimensional microstructured tissue scaffolds fabricated by two-photon laser scanning photolithography *Biomaterials* **31** 7648–52
[8] Elomaa L, Teixeira S, Hakala R, Korhonen H, Grijpma D W and Seppälä J V 2011 Preparation of poly(ε-caprolactone)-based tissue engineering scaffolds by stereolithography *Acta Biomater.* **7** 3850–6
[9] Melchels F P W, Feijen J and Grijpma D W 2009 A poly(d,l-lactide) resin for the preparation of tissue engineering scaffolds by stereolithography *Biomaterials* **30** 3801–9
[10] Timashev P *et al* 2016 Novel biodegradable star-shaped polylactide scaffolds for bone regeneration fabricated by two-photon polymerization *Nanomedicine* **11** 1041–53
[11] Fukushima K 2016 Poly(trimethylene carbonate)-based polymers engineered for biodegradable functional biomaterials *Biomater. Sci.* **4** 9–24
[12] Ajami A, Husinsky W, Tromayer M, Gruber P, Liska R and Ovsianikov A 2017 Measurement of degenerate two-photon absorption spectra of a series of developed two-photon initiators using a dispersive white light continuum Z-scan *Appl. Phys. Lett.* **111** 071901
[13] Ren T, Steiger W, Chen P, Ovsianikov A and Demirci U 2020 Enhancing cell packing in buckyballs by acoustofluidic activation *Biofabrication* **12** 025033
[14] Weiß T, Berg A, Fiedler S, Hildebrand G, Schade R, Schnabelrauch M and Liefeith K 2009 *IFMBE Proceedings* vol 25/10 (Berlin: Springer)
[15] Zandrini T, Shan O, Parodi V, Cerullo G, Raimondi M T and Osellame R 2019 Multi-foci laser microfabrication of 3D polymeric scaffolds for stem cell expansion in regenerative medicine *Sci. Rep.* **9** 11761
[16] Koroleva A V, Guseva D S, Konovalov N A, Zharikova T M, Ponimaskin E G, Chichkov B N, Bagratashvili V N and Timashev P S 2016 Polylactide-based biodegradable scaffolds fabricated by two-photon polymerization for neurotransplantation *Sovrem. Tehnol. Med.* **8** 23–28

[17] Claeyssens F et al 2009 Three-dimensional biodegradable structures fabricated by two-photon polymerization *Langmuir* **25** 3219–23
[18] Trautmann A, Rüth M, Lemke H D, Walther T and Hellmann R 2018 Two-photon polymerization based large scaffolds for adhesion and proliferation studies of human primary fibroblasts *Opt. Laser Technol.* **106** 474–80
[19] Danilevicius P, Georgiadi L, Pateman C J, Claeyssens F, Chatzinikolaidou M and Farsari M 2015 The effect of porosity on cell ingrowth into accurately defined, laser-made, polylactide-based 3D scaffolds *Appl. Surface Sci.* **336** 2–10
[20] Gittard S D, Nguyen A, Obata K, Koroleva A, Narayan R J and Chichkov B N 2011 Fabrication of microscale medical devices by two-photon polymerization with multiple foci via a spatial light modulator *Biomed. Opt. Express* **2** 3167
[21] Koroleva A, Gill A A, Ortega I, Haycock J W, Schlie S, Gittard S D, Chichkov B N and Claeyssens F 2012 Two-photon polymerization-generated and micromolding-replicated 3D scaffolds for peripheral neural tissue engineering applications *Biofabrication* **4** 2
[22] Mačiulaitis J et al 2015 Preclinical study of SZ2080 material 3D microstructured scaffolds for cartilage tissue engineering made by femtosecond direct laser writing lithography *Biofabrication* **7** 015015
[23] Paun I A et al 2018 Laser-direct writing by two-photon polymerization of 3D honeycomb-like structures for bone regeneration *Biofabrication* **10** 025009
[24] Schade R, Weiß T, Berg A, Schnabelrauch M and Liefeith K 2010 Two-photon techniques in tissue engineering *Int. J. Artif. Organs* **33** 219–27
[25] Trautmann A, Götzendorfer B, Walther T and Hellmann R 2018 Scaffolds in a shell–a new approach combining one-photon and two-photon polymerization *Opt. Express* **26** 29659
[26] Pollack S et al 2019 Polymer-based additive manufacturing: historical developments, process types and material considerations *Polymer-Based Additive Manufacturing* (Berlin: Springer) pp 1–22
[27] Schafer K J, Hales J M, Balu M, Belfield K D, Van Stryland E W and Hagan D J 2004 Two-photon absorption cross-sections of common photoinitiators *J. Photochem. Photobiol.* A **162** 497–502
[28] Zandrini T, Shan O, Parodi V, Cerullo G, Raimondi M T and Osellame R 2019 Multi-foci laser microfabrication of 3D polymeric scaffolds for stem cell expansion in regenerative medicine *Sci. Rep.* **9** 1–9
[29] Yang L, El-Tamer A, Hinze U, Li J, Hu Y, Huang W, Chu J and Chichkov B N 2015 Parallel direct laser writing of micro-optical and photonic structures using spatial light modulator *Opt. Lasers Eng.* **1** 26–32
[30] Loh Q L and Choong C 2013 Three-dimensional scaffolds for tissue engineering applications: role of porosity and pore size *Tissue Eng.* B **19** 485–502
[31] Katoh K, Tanabe T and Yamauchi K 2004 Novel approach to fabricate keratin sponge scaffolds with controlled pore size and porosity *Biomaterials* **25** 4255–62
[32] Thomson R C, Shung A K, Yaszemski M J and Mikos A G 2000 Polymer scaffold processing. *Principles of Tissue Engineering* (Amsterdam: Elsevier) pp 251–62
[33] Murphy C M, Haugh M G and O'Brien F J 2010 The effect of mean pore size on cell attachment, proliferation and migration in collagen-glycosaminoglycan scaffolds for bone tissue engineering *Biomaterials* **31** 461–6
[34] Mygind T, Stiehler M, Baatrup A, Li H, Zou X, Flyvbjerg A, Kassem M and Bünger C 2007 Mesenchymal stem cell ingrowth and differentiation on coralline hydroxyapatite scaffolds *Biomaterials* **28** 1036–47
[35] Kuboki Y, Jin Q and Takita H 2001 Geometry of carriers controlling phenotypic expression in BMP-induced osteogenesis and chondrogenesis *J. Bone Joint Surg. Am.* **83**
[36] Oh S H, Kim T H, Il I G and Lee J H 2010 Investigation of pore size effect on chondrogenic differentiation of adipose stem cells using a pore size gradient scaffold *Biomacromolecules* **11** 1948–55
[37] Bružauskaitė I, Bironaitė D, Bagdonas E and Bernotienė E 2016 Scaffolds and cells for tissue regeneration: different scaffold pore sizes—different cell effects *Cytotechnology* **68** 355–69
[38] Do C H, Hong J M, Kang T-Y, Jung J W, Ha D-H and Cho D-W 2012 Effects of micro-patterns in three-dimensional scaffolds for tissue engineering applications *J Micromech. Microeng.* **22** 125002
[39] Schizas C and Karalekas D 2011 Mechanical characteristics of an Ormocomp® biocompatible hybrid photopolymer *J. Mech. Behav. Biomed. Mater.* **4** 99–106
[40] Schlie S, Ngezahayo A, Ovsianikov A, Fabian T, Kolb H A, Haferkamp H and Chichkov B N 2007 Three-dimensional cell growth on structures fabricated from ORMOCER® by two-photon polymerization technique *J. Biomater. Appl.* **22** 275–87
[41] Guillaume O, Geven M A, Grijpma D W, Tang T T, Qin L, Lai Y X, Yuan H, Richards R G and Eglin D 2016 Poly(trimethylene carbonate) and nano-hydroxyapatite porous scaffolds manufactured by stereolithography *Polym. Adv. Technol.* **28** 1219–25
[42] Guo Z, Grijpma D W and Poot A A 2017 Preparation and characterization of flexible and elastic porous tubular PTMC scaffolds for vascular tissue engineering *Polym. Adv. Technol.* **28** 1239–44
[43] van Bochove B, Hannink G, Buma P and Grijpma D W 2016 Preparation of designed poly(trimethylene carbonate) meniscus implants by stereolithography: challenges in stereolithography *Macromol. Biosci.* **16** 1853–63
[44] Melissinaki V, Gill A A, Ortega I, Vamvakaki M, Ranella A, Haycock J W, Fotakis C, Farsari M and Claeyssens F 2011 Direct laser writing of 3D scaffolds for neural tissue engineering applications *Biofabrication* **3**
[45] Guillaume O et al 2017 Surface-enrichment with hydroxyapatite nanoparticles in stereolithography-fabricated composite polymer scaffolds promotes bone repair *Acta Biomater.* **54** 386–98
[46] Guillaume O et al 2020 Orbital floor repair using patient specific osteoinductive implant made by stereolithography *Biomaterials* **233** 119721
[47] Barradas A, Yuan H, van Blitterswijk C and Habibovic P 2011 Osteoinductive biomaterials: current knowledge of properties, experimental models and biological mechanisms *Eur. Cells Mater.* **21** 407–29
[48] Werner M, Blanquer S B G, Haimi S P, Korus G, Dunlop J W C, Duda G N, Grijpma D W and Petersen A 2017 Surface curvature differentially regulates stem cell migration and differentiation via altered attachment morphology and nuclear deformation *Adv. Sci.* **4** 1600347
[49] McCullen S D, Autefage H, Callanan A, Gentleman E and Stevens M M 2012 Anisotropic fibrous scaffolds for articular cartilage regeneration *Tissue Eng.* A **18** 2073–83
[50] Yousefi A-M, Hoque M E, Prasad RGS V and Uth N 2015 Current strategies in multiphasic scaffold design for osteochondral tissue engineering: A review *J. Biomed. Mater. Res.* A **103** 2460–81